

Stable magnetic fields in stellar interiors

J. Braithwaite^{1,3} and Å. Nordlund^{2,4}

¹ Max-Planck-Institut für Astrophysik, Karl-Schwarzschild-Straße 1, Postfach 1317, D-85741 Garching, Germany

² Department of Astrophysics, Niels Bohr Institute, Juliane Maries Vej 30, 2100 København Ø, Denmark

³ jon@mpa-garching.mpg.de, ⁴ aake@astro.ku.dk

the date of receipt and acceptance should be inserted later

Abstract. We investigate the 50-year old hypothesis that the magnetic fields of the Ap stars are stable equilibria that have survived in these stars since their formation. With numerical simulations we find that stable magnetic field configurations indeed appear to exist under the conditions in the radiative interior of a star. Confirming a hypothesis by Prendergast (1956), the configurations have roughly equal poloidal and toroidal field strengths. We find that tori of such twisted fields can form as remnants of the decay of an unstable random initial field. In agreement with observations, the appearance at the surface is an approximate dipole with smaller contributions from higher multipoles, and the surface field strength can increase with the age of the star. The results of this paper were summarised by Braithwaite & Spruit (2004).

Key words. instabilities – magnetohydrodynamics (MHD) – stars: magnetic fields

1. Introduction

The peculiar A and B stars (Ap-Bp) are main-sequence stars with a strong surface magnetic field. The nature of these fields has been the subject of a debate that has accompanied the development of astrophysical magnetohydrodynamics since the 1950's. The two leading possibilities were the 'fossil field' theory (Cowling 1945) and the core dynamo theory. The fossil field theory appears to be supported by some observations, such as the very high strength of the field in some stars, the apparent stationary state of the field and the wide range of field strengths observed.

The main problem of the theory has always been the difficulty of finding realistic equilibrium configurations for star-like objects with the analytic methods available, and of demonstrating the stability of such configurations. With increasing computing power, important aspects of this problem are now accessible by purely numerical means. While numerical results for the present problem cannot match the precision of analytic methods, they are excellent at providing clues about the kinds of magnetic configurations that might exist, or to estimate the likelihood that the hypothesised stable fields can exist at all.

In this paper we present numerical results that make the fossil field theory very plausible, by showing that field configurations of a well-defined type appear to develop naturally by the decay of stronger unstable fields. We begin with a brief summary of the relevant observational properties of the magnetic stars.

1.1. History and properties of the Ap-Bp stars

Maury (1897) noted that the spectrum of α^2 CVn (one of the brightest of this class, at magnitude 2.9) was peculiar, showing unusual weakness of the K line and strength of the Si II doublet at 4128Å. Variability of some of the lines was subsequently discovered and Belopolsky (1913) measured the changes in intensity and radial velocity of one of the lines (Eu at 4129Å), finding a period of 5.5 days. The photometric light curve was measured (Guthnick & Prager 1914) and similar behaviour was later found in other Ap stars (for instance Morgan 1933 and Deutsch 1947).

Only upon the discovery of variable magnetic fields (Babcock 1947) did any explanation of this interesting spectral behaviour become possible. It was found that Ap stars have an unusually strong magnetic field, with surface strengths ranging from a few hundred to a few tens of thousand gauss. The variability of the field can be most easily explained by imagining a static field not symmetrical about the rotation axis; the spectral peculiarity is then taken to be a consequence of the effect the magnetic field has on the transport of chemical species.

Various techniques have been developed to observe the magnetic field on the surface of stars. Measurement of the circular polarisation of the spectral lines is used to give an average (weighted towards the centre of the disc) of the line-of-sight component of the surface field, called the *longitudinal field* in the literature. In some stars with slow rotation (and hence small Doppler broadening) spectral lines are split into separate Zeeman components, in which case an average over the disc of the modulus of the field can be obtained: this is called the *field modulus*. If one were to do this on the Sun, one would find that

the longitudinal field were extremely small in comparison to the modulus. This is because the field has a small scale structure, and the positive and negative regions of the line-of-sight component cancel each other out. If one makes this observation of a magnetic Ap star, this is not the case – implying a large scale structure. It is our task to find an explanation for the strong, large-scale fields of Ap stars.

In addition to the longitudinal field and the field modulus, two more quantities can readily be measured: the *quadratic field* and the *crossover field*. The former quantity is approximately proportional to $(\langle B^2 \rangle + \langle B_z^2 \rangle)^{1/2}$, where B_z is the line-of-sight component, and the latter is given by $v \sin i \langle x B_z \rangle$, where x is the normalised distance from the stellar rotation axis in the plane of the sky. (Mathys 1995a, Mathys 1995b). This set of ‘observables’ can be used to model the field on the stellar surface – one constructs a model whose free parameters are made to converge on a solution by finding the point of minimum disagreement with observations.

Various models for the field configuration have been tried. The simplest assume an axisymmetric field, inclined with respect to the rotation axis (e.g. Landstreet & Mathys 2000). More elaborate models are those of Bagnulo et al. (2002), which assumes a field with dipole and quadrupole components at arbitrary orientations, and the point-field-source model of Gerth et al. (1997). One thing that all these models have in common is that they fail, in many stars, to describe the observations accurately. This implies a more complex field structure than can be written as the sum of low-order spherical harmonics. On the other hand it is often found that parameter space contains several χ^2 minima so it is not clear which one of these configurations, if any, represents reality. Despite this, many of the results obtained do seem to be reasonably model-independent. A more sophisticated approach which can yield better results is that of *Zeeman-Doppler Imaging* (see Piskunov & Kochukhov 2002), which has as of yet only been applied to a very small number of stars, owing to the high quality of the spectra required.

It has been suggested that Ap stars are all above a certain age – Hubrig et al. (2000a) placed Ap stars on the H-R diagram and found none in the first 30% of their main sequence lifetimes. It is possible that some dynamo process only begins at a certain time, perhaps as the size of the radiative core changes (an A star has a radiative envelope and a convective core); it is also possible that the Ap progenitor contains a strong field in its interior which only appears at the surface at some evolutionary stage. However, this result does contradict some earlier results (North 1993; Wade 1997) which claim that Ap stars are distributed uniformly across the width of the main sequence band.

The rotation period of Ap stars tends to be longer than in normal A stars (Bonsack & Wolff 1980). Whether the young Ap progenitors betray their destiny though a similarly long period is unclear; authors on the subject have yet to reach a definite conclusion (see, for instance, Hubrig et al. 2000b) and await observations more numerous than have so far been undertaken.

Landstreet & Mathys (2000) find that the magnetic axis of slowly-rotating ($P > 25$ days) Ap stars is overwhelmingly

more likely to be close to the rotation axis than one would expect from a random distribution – of their sample of 16 stars, 14 have the two axes within 30° of each other, the other two between 30° and 45° . This result, which was obtained using the best-fit method with an axisymmetric field model, is reassuringly confirmed by Bagnulo et al. (2002) who use a field consisting of dipole and quadrupole at arbitrary orientation. The rapidly-rotating ($P < 25$ days) stars, however, show no such alignment – the statistics are consistent with a random orientation of the magnetic axis in relation to the rotation axis.

2. Nature of the magnetic field in Ap stars

The question of how the structure of a star can accommodate a magnetic field, and if it can survive on a time-scale as long as the the main sequence lifetime has accompanied the early development of astrophysical MHD (e.g. Cowling 1958, Chandrasekhar 1961, Roberts 1967; the topic is reviewed in Borra, Landstreet & Mestel 1982). The question has two parts: equilibrium and stability.

2.1. Equilibrium

Finding equilibrium configurations of stars with magnetic fields turns out to be a mostly technical problem. Though early efforts, concentrating on ‘analytical solutions’, had limited success, this does not imply a conceptual problem affecting the existence of magnetic equilibria. Construction of equilibria by numerical methods has become an accepted approach (e.g. Bonazzola et al. 1993).

For a dynamical equilibrium, there has to be a balance between the pressure gradient, gravity and the Lorentz force. The Lorentz force is generally not a conservative force, hence cannot be balanced by the pressure gradient alone. Gravity, or more accurately buoyancy forces, must be involved in maintaining equilibrium. For a given magnetic field configuration, it is in general possible to find a (slightly distorted) stellar model that will balance the magnetic forces throughout the star. To see this (without actual proof), note that the three components of a magnetic field can in general be described in terms of two scalar fields (since $\text{div} \mathbf{B} = 0$ takes care of one degree of freedom). Hence the magnetic force can also be described in terms of two degrees of freedom only. Ignoring thermal diffusion, the thermodynamic state of the gas has two degrees of freedom (pressure and entropy, for example). Where the magnetic field is sufficiently weak (in the sense $B^2/(8\pi P) \ll 1$), equilibrium therefore can be obtained, for a given magnetic configuration, by suitable small adjustments of the pressure and entropy distributions. An exception occurs in convectively unstable layers, which do not support significant differences in entropy.

Where the field strength is not small in this sense, for example in the atmosphere of the star, not all field configurations are possible, and the magnetic field must instead be close to a force-free configuration. Conceptually, we can thus divide a radiatively stratified star into an interior where any field configuration is allowed (if adiabatic equilibrium is the only concern, and up to some maximum strength), and an atmosphere

containing a nearly force-free field. The two join somewhere around the surface where $B^2/(8\pi P) = 1$.

Deviations from magnetic equilibrium travel through the star at the Alfvén speed. Even if the magnetic field in the interior is weak ($B^2/(8\pi P) \ll 1$), the corresponding adjustment time can still be very short compared to the age of the star, since this is so many orders of magnitude longer than the dynamical time-scale of a star (of the order 10^{11} times longer, for a main sequence A-star). For a field of 1000 G in an Ap star, for example, the Alfvén crossing time is of the order 10 years, a fraction 10^{-8} of the star’s main sequence life.

In our calculations, the laborious process of producing magnetic equilibria by explicit construction from the equilibrium equations is replaced by the ‘brute force’ method of following the evolution of the configuration in a time dependent manner. Though less elegant, it is simpler to implement and has the additional advantage of addressing at the same time the stability of the field.

2.2. Stability

The (dynamic) stability of an equilibrium is equally important, since instability will result in changes on the same (Alfvén) time-scale. Gravity (buoyancy) is a strongly stabilising force on the field in a radiative stellar interior, preventing displacements in the radial direction. But in the two horizontal directions (along an equipotential surface), there is essentially no stabilising force. Is stabilisation in one direction sufficient for overall stability of magnetic equilibria in stars? What do such equilibria look like if they exist? This question has been the subject of a significant amount of analytic work done throughout the last fifty years.

Taylor (1973) looked at toroidal fields in stars, that is, fields that have only an azimuthal component B_ϕ in some spherical coordinate frame (r, θ, ϕ) with the origin at the centre of the star. With the energy method, he derived necessary and sufficient stability conditions for adiabatic conditions (no viscosity, thermal diffusion or magnetic diffusion). The main conclusion was that such purely toroidal fields are always unstable at some place in the star, in particular to perturbations of the $m = 1$ form, and that stability at any particular place does not depend on field strength but only on the form of the field. An important corollary of the results in this paper (esp. the Appendix) was the proof that instability is *local* in meridional planes. If the necessary and sufficient condition for instability is satisfied at any point (r, θ) , there is an unstable eigenfunction that will fit inside an infinitesimal environment of this point. The instability is always global in the azimuthal direction, however. The instability takes place in the form of a low-azimuthal order displacement in a ring around the star. Connected with this is the fact that the growth time of the instability is of the order of the time it takes an Alfvén wave to travel around the star on a field line.

The opposite case is a field in which all field lines are in meridional planes ($B_\phi = 0$, see Fig. 1). In subsequent papers Markey & Tayler (1973, 1974) and independently Wright (1973) studied the stability of axisymmetric poloidal fields in

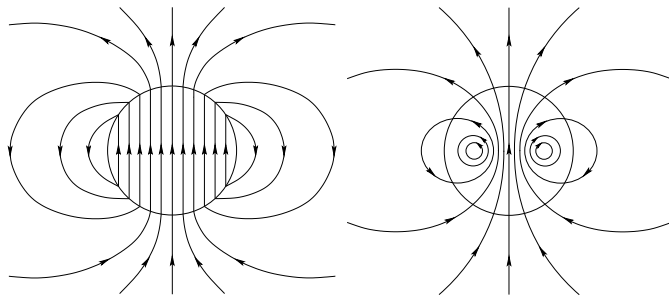


Fig. 1. Poloidal field configurations. Left: all field lines close outside the star, this field is unstable by an argument due to Flowers & Ruderman. For the case where some field lines are closed inside the star, instability was proven by Wright and Markey & Tayler.

which (at least some) field lines are closed within the star (right-hand side of Fig. 1). These fields were again found to be unstable.

A case not covered by these analyses was that of a poloidal field in which *none* of the field lines close within the star. An example of such a field is that of a uniform field inside, matched by a dipole field in the vacuum outside the star (left-hand side of Fig. 1). This case has been considered earlier by Flowers & Ruderman (1977) who found it to be unstable, by the following argument. Consider what would happen to such a dipolar field if one were to cut the star in half (along a plane parallel to the magnetic axis), rotate one half by 180° , and put the two halves back together again. The magnetic energy inside the star would be unchanged, but in the atmosphere, where the field can be approximated by a potential field, i.e. with no current, the magnetic energy will be lower than before. This process can be repeated *ad infinitum* – the magnetic energy outside the star approaches zero and the sign of the field in the interior changes between thinner and thinner slices.

The reduction of the external field energy is responsible for driving the instability. Since the initial external field energy is of the same order as the field energy inside the star, the initial growth time of the instability is of the order of the Alfvén travel time through the star, as in the cases studied by Markey & Tayler and Wright.

Prendergast (1956) showed that an equilibrium can be constructed from a linked poloidal-toroidal field, but stopped short of demonstrating that this field could be stable. Since both purely toroidal fields and purely poloidal field are unstable, a stable field configuration, if one exists, must apparently be such a linked poloidal-toroidal shape. Wright (1973) showed that a poloidal field could be stabilised by adding to it a toroidal field of comparable strength. However, the result was again somewhat short of a proof.

Kamchatnov (1982) constructed an equilibrium field, which he claimed was stable. It has the following form:

$$\begin{aligned} B_x &= \frac{2(xz - y)}{(1 + r^2)^3} \\ B_y &= \frac{2(yz - x)}{(1 + r^2)^3} \end{aligned} \quad (1)$$

$$B_z = \frac{1 + 2z^2 - r^2}{(1 + r^2)^3}$$

where x , y and z are unitless Cartesian coordinates, and $r^2 = x^2 + y^2 + z^2$. To be in equilibrium, this field has to be accompanied by a velocity field of similar form. The field is a twisted torus; if one started with a hoop of field lines (i.e. a toroidal field), cut the hoop at one point, and twisted one end 360° and reconnected the two ends again (so that each field line connects back to itself), one would get something like the field described by the equations above.

These results were all valid only in the absence of dissipative effects. The damping due to such effects might be expected to result in a somewhat increased stability. The only case in which dissipative effects have been investigated in detail is that of a purely toroidal field. Acheson's (1978) analysis exploits the local nature of the instability process in this case to include the effects of viscosity, magnetic and thermal diffusion. Because of the low values of these coefficients in a stellar interior, stabilisation is found to occur only at very low field strengths, well below those observed in Ap/Bp stars.

The effect of rotation was investigated by Pitts & Tayler (1986) for the adiabatic case. These authors arrived at the conclusion that although some instabilities could be inhibited by sufficiently rapid rotation, other instabilities were likely to remain, whose growth could only be slowed by rotation – the growth timescale would still be very short compared to a star's lifetime. It seems that a toroidal field could be stabilised by rotation above a certain speed if the rotation and magnetic axes were parallel. However, there are generally likely to be other instabilities which survive even rapid rotation, albeit at a rate reduced by a factor σ_0/Ω where σ_0 is the growth rate in the absence of rotation. They did not however exclude the possibility that rotation at a large angle to the magnetic axis of symmetry could stabilise a mainly poloidal field.

This was one of the last papers on the subject to use purely analytic methods – the problem had become so complicated that no more definite conclusions could be made. Numerical simulations were recently used to look at the stability of toroidal fields (Braithwaite 2005); it was demonstrated that such a field is subject to an instability growing on an Alfvén-crossing time-scale, which could be suppressed by rotation of an axis parallel to the magnetic axis. These simulations were done in a localised basis – a small section of the radiative envelope on the magnetic axis was modelled. To look at the stability of more general field configurations, it is necessary to model an entire star.

In the calculations reported below the stability problem is not studied separately; any configuration that survives the dynamical evolution of a given initial state will be a stable field, on the time-scales that can be followed numerically. The evolution can typically be followed for a few hundred Alfvén crossing times; surviving fields are therefore of the dynamically stable type sought.

It is possible that the outcome depends on the initial conditions, which could of course explain why some A stars are magnetic and others are not. A second goal is thus to find clues

as to the initial conditions set at the time of formation of a magnetic A star.

3. The numerical model

The star is modelled on a Cartesian grid. For a spherical object like a star this might sound unnatural. Alternatives like cylindrical or spherical coordinates are more natural for analytical methods, but are known to produce serious artefacts in numerical simulations because of the coordinate singularities. Cartesian coordinates are the simplest to implement and have a low computing cost per grid point. A disadvantage is that the computational box must be taken somewhat larger than the star studied, which increases computing effort again.

The boundary conditions used are periodic in all directions. Such conditions are easy to implement and minimise boundary artefacts.

The equation of state is that of an ideal gas with a fixed ratio of specific heats $\gamma = 5/3$. The gravitational potential is determined consistently with the non-magnetic state of the star, but thereafter kept fixed at this value during the evolution of the magnetic field (the Cowling approximation).

It should be stressed that the star modelled here is non-rotating. This is no problem for slowly-rotating Ap stars where the Alfvén time-scale is much shorter than the rotational time-scale; in the faster-rotating Ap stars, since rotation tends to suppress magnetic instabilities, the effect of the rotation on any stable field configuration is likely to be one of orientation only. This is confirmed by the observations mentioned in the introduction (Landstreet & Mathys 2000) – that the only difference between the slow-rotators and the fast-rotators is the angle between the rotation and magnetic axes.

3.1. Treatment of the atmosphere

As the Flowers-Ruderman argument shows, instability of the field can be driven by the magnetic energy in the volume outside the star. The calculations therefore must include a mechanism to allow magnetic energy release in the atmosphere. The atmosphere is magnetically dominated ($\beta \ll 1$) and has something close to a potential field, as no large currents can exist there. In principle, the code will reproduce this automatically, since magnetic diffusion (whether numerical or explicitly included) will allow reconnection of field lines in the atmosphere in response to changes at the surface driven by the dynamics of the magnetic field in the interior.

When numerically modelling this, however, problems arise because the Alfvén speed becomes very large in an atmosphere that is modelled sufficiently realistically to allow reconnection to take place rapidly enough. This causes the time step to drop below acceptable values.

By including a large electrical resistivity in the atmosphere, the field can be kept close to a potential field irrespective of the Alfvén speed. Thus in the induction equation a magnetic diffusivity, η_a , is included, whose value is zero in the stellar interior and constant in the atmosphere (with a transition zone located between the same radii as the temperature transition zone visible in Fig. 3). The corresponding heating term in the energy

equation is left out since the diffusivity is artificial, and atmospheric heating can not be treated realistically anyway without also including the compensating radiative loss terms.

3.2. Time-scales and computational practicalities

Three different time-scales play a role in the numerics of the problem: the sound travel time $t_s = R_*/c_s$, the Alfvén crossing time $t_A = R_*/v_A$ and the Ohmic diffusion time $t_d = R_*^2/\eta$. In a real star (assuming a field strength ~ 1000 G), these differ by ratios of the order $t_A/t_s \sim 10^4$, $t_d/t_s \sim 10^{10}$. Such ratios are well outside the dynamic range accessible numerically.

In the main problem addressed in this study, namely the approach of a field configuration to an equilibrium state and the stability of this state, the governing time-scale is the Alfvén travel time. The hydrostatic adjustment of the star to a changing field configuration happens on the much shorter sound crossing time, hence the evolution of the field does not depend explicitly on the sound crossing time, but only on the Alfvén speed. An overall change in the field strength is thus almost equivalent to a change in time scale. We exploit this by using high field strengths, such that $t_A/t_s \sim 10$, a value close to the maximum for which the dynamics can plausibly be expected to be nearly independent of the sound travel time.

In some calculations, the evolution of a dynamically stable field configuration in the presence of an explicit magnetic diffusion is studied (see Sect. 7.3). In these cases, both the dynamic and the diffusive time-scales must be followed. The two can be separated only if the diffusive time-scale is sufficiently long compared with the Alfvén time. For these cases, the diffusivity is adjusted such that the diffusive time scale was longer by a factor of order 10; hence these calculations are also of the order 10 times as demanding as the calculations that only follow the Alfvén time scale.

3.3. Acceleration of the code by rescaling

During the evolution of the field from an arbitrary or unstable configuration, its amplitude decreases by large factors. Following the intrinsic development as the Alfvén time-scale increases becomes increasingly expensive, limiting the degree of evolution that can be followed. To circumvent this problem, a routine was added to the code which increases the strength of the magnetic field (uniformly throughout the entire computational box) to keep the total magnetic energy constant. The code then keeps a record of how fast the magnetic field would have decayed in the absence of this routine. This information is then used to reconstruct the time axis and the field amplitude as a function of time. We call this numerical device *amplitude rescaling*. It can be shown to give exact results in the case when the Alfvén speed is the only relevant signal speed. In practice, this means we expect it to give a good approximation for the evolution of the field configuration when the Alfvén crossing time is much longer than the sound crossing time but much shorter than the diffusive time, i.e. in the limiting case $\eta/R_* \ll V_A \ll c_s$. Tests were done to make sure that the evolution of the field is indeed largely unaffected by this pro-

cedure (Sect. 7.1.) The procedure is useful even in cases where the separation of Alfvén, sound and diffusive time scales is not as clean. If we are interested mainly in the stable *final equilibrium configuration*, it is sufficient to have a numerical procedure that finds this equilibrium efficiently and the accuracy of the evolution to this equilibrium is of less concern. This applies in essence to most of the results reported here.

The model does not include thermal processes such as production of heat in the core and transport to the surface, and Ohmic heating from electrical currents; the latter would be nonsensical anyway as a result of the rescaling of the magnetic field. Because of this, and because the star is not rotating, we do not expect the results to give us useful information about flows in the stellar interior.

4. The numerical code

We use a three-dimensional MHD code developed by Nordlund & Galsgaard (1995), written in Cartesian coordinates. The code uses a staggered mesh, so that variables are defined at different points in the gridbox. For example, ρ is defined in the centre of each box, but u_x in the centre of the face perpendicular to the x-axis, so that the value of x is lower by $\frac{1}{2}dx$. Interpolations and spatial derivatives are calculated to fifth and sixth order respectively. The third order predictor-corrector time-stepping procedure of Hyman (1979) is used.

The high order of the discretisation is a bit more expensive per grid point and time step, but the code can be run with fewer grid points than lower order schemes, for the same accuracy. Because of the steep dependence of computing cost on grid spacing (4th power for explicit 3D) this results in greater computing economy.

For stability, high-order diffusive terms are employed. Explicit use is made of highly localised diffusivities, while retaining the original form of the partial differential equations.

The code conserves $\nabla \cdot \mathbf{B}$ only up to machine accuracy. For previous applications this was no problem as the code was run for shorter lengths of time. For this application, however, we are modelling a star over many Alfvén timescales, and accumulation of machine errors became a problem. An additional routine was required to remove the component of the field with non-zero divergence. This was done by periodically (every few hundred timesteps) expressing the field as the gradient of a scalar and the curl of a vector, the former then being deleted.

5. Initial conditions

We begin all of the simulations with the spherically symmetrical density and temperature profiles of polytropic star where $P \propto \rho^{1+1/n}$. A value of $n = 3$ was chosen, as it is fairly typical of the non-convective stellar envelope of A stars – half-way between the isothermal ($n = \infty$) and convective ($n = 3/2$) cases. This polytrope is truncated at a distance R_* , the radius of the simulated star, and the region outside this replaced by a hot atmosphere, with a temperature about half that at the centre of the star. The surface density of the polytrope is of the order 0.002 of the central density; a smaller value of the surface den-

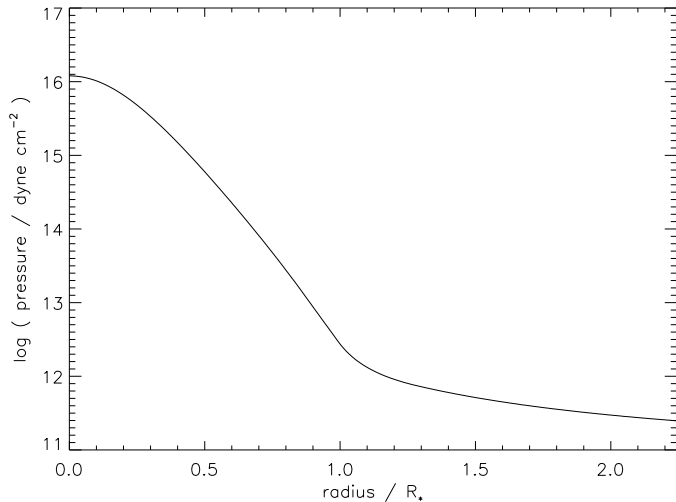


Fig. 2. Pressure vs. radius of the model star at $t = 0$.

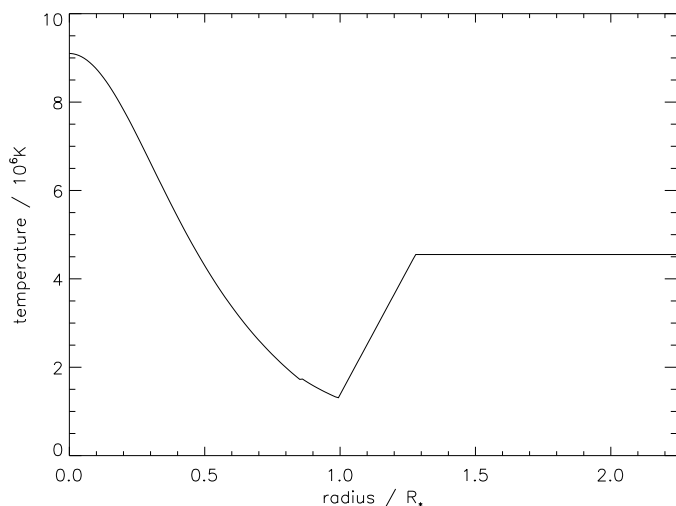


Fig. 3. Temperature vs. radius of the model star at $t = 0$.

sity is numerically impractical because of the very high Alfvén speeds that would result in the atmosphere.

If we choose to specify the mass M_* , radius R_* and mean molar mass μ of the star as $2M_\odot$, $1.8R_\odot$ and 0.6 g mol^{-1} (typical A-star values), then the central temperature is $9 \times 10^6 \text{ K}$ with a polytrope of this index. The computational box is a cube of side $4.5R_*$.

Figs. 2 and 3 show the pressure and temperature profiles.

Nothing is known about the magnetic configuration produced during star formation. As a way of expressing this ignorance, we have started the series of calculations with a set of cases with random initial fields. A magnetic vector potential was set up as a random field containing spatial frequencies up to a certain value (so that the length scales were at least a few grid spacings). The result was then multiplied by

$$\exp(-r^2/r_m^2), \quad (2)$$

so that the field strength in the atmosphere was negligible. The magnetic field was then calculated from this vector potential. The strength of the field was normalised to be strong enough to allow things to happen on computationally conve-

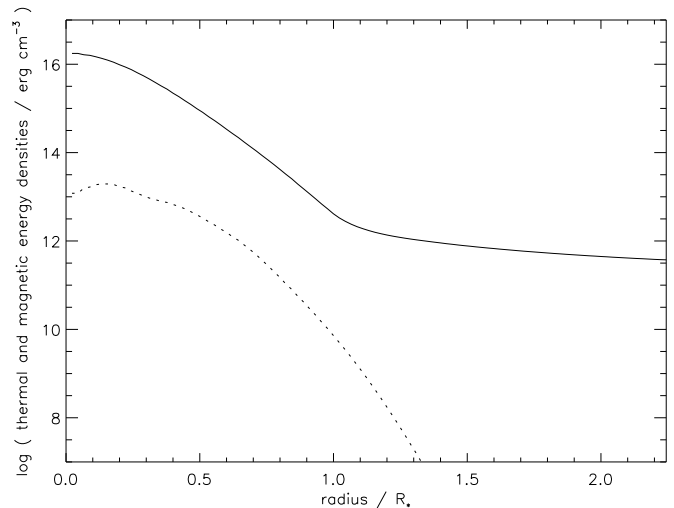


Fig. 4. Thermal (solid line) and magnetic (dotted line) energy densities at $t = 0$, averaged over horizontal surfaces, as a function of radius. The variations of magnetic energy density with radius reflect the particular realisation of the random initial field.

nient timescales whilst holding to the condition that the magnetic energy be much less than the thermal. The value of β (thermal over magnetic energy density) in the stellar interior was therefore set to around 100 at the beginning of the simulation. The total magnetic energy is equal to $1.2 \times 10^{46} \text{ erg}$ – this corresponds to a mean field of around $5 \times 10^6 \text{ gauss}$, a factor of between 200 and 20,000 greater than the fields observed on the *surface* of Ap stars. The Alfvén timescale, 0.6 days, will therefore also be shorter by this factor than one might expect in reality.

Fig. 4 shows the thermal and magnetic energy densities as a function of radius for one particular realisation of the random initial conditions. The difference between these two lines gives a measure of β , which is typically 100 in the interior, tending to infinity in the atmosphere. Perhaps more relevant though than the ratio of the energy densities is the ratio of sound and Alfvén speeds; these two speeds are shown in Fig. 5.

6. Visualising the results

One of the greatest difficulties in any numerical study of magnetic fields is the visualisation of the results. A number of techniques have been used in this study. One of the most useful pieces of software was found to be IRIS Explorer, which allows user-defined procedures to easily be added to a pre-existing set of 3-D rendering modules. For most of the renderings shown here we use a combination of user-defined and pre-existing modules that combines projections of three-dimensional field lines and surfaces. A field line projection routine has been used which picks starting points, either at random throughout the whole computational box (biased in favour of regions of high field strength) or around a certain point, and then traces the field from these points until the field strength drops below a certain value.

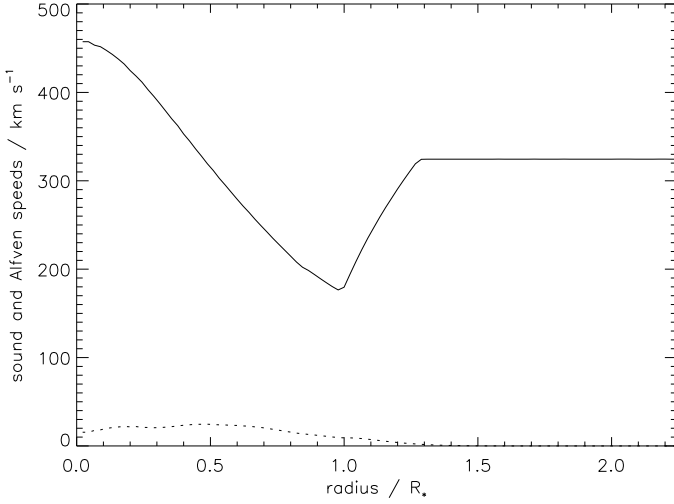


Fig. 5. Sound (solid line) and Alfvén (dotted line) speeds at $t = 0$.

Plotting field lines alone can produce a rather chaotic picture, as it is not obvious at what depth each line lies. To complement the lines, it is useful to plot an opaque surface of constant radius to provide a background. This surface can then be shaded according to the sign of the normal field component. A plot of this form can be seen in Fig. 20 (the four large frames in this figure).

It is also helpful to be able to see the axis of symmetry of the magnetic field. We define the magnetic axis \mathbf{M} in the following way:

$$\mathbf{M} = \oint_{r=R_*} (\mathbf{B} \cdot \hat{\mathbf{r}}) \mathbf{r} dS, \quad (3)$$

The arrow representing this axis has been added to the snapshots in Fig. 20.

The stable magnetic field configurations found here generally have the form of tori. To visualise their shape, something is needed to show them as surfaces or nested surfaces. Field lines are needed too, but bundles of field lines alone are much too confusing, while iso-surfaces of field strength are too insensitive to the topological properties of the configuration.

A useful visual aid which helps to highlight the position of the torus field is created as follows. A scalar field C is calculated, which is equal to the radius of curvature:

$$C = \frac{B^3}{|\mathbf{B} \times \mathbf{A}|} \quad \text{where} \quad \mathbf{A} = (\mathbf{B} \cdot \nabla) \mathbf{B}. \quad (4)$$

This alone is not the ideal field to highlight the torus, as it fails to distinguish the core of a torus from the field lines which go through the middle of the star and emerge at either end. It is therefore necessary to look at the direction of this radius of curvature – we are interested principally in places where it is parallel to the radius vector \mathbf{r} . Hence the dot product of the unit position vector and the radius-of-curvature vector \mathbf{C} is calculated, giving a scalar field F :

$$F = \hat{\mathbf{r}} \cdot \mathbf{C} \quad \text{where} \quad \mathbf{C} = \frac{B^2 \mathbf{A} - (\mathbf{A} \cdot \mathbf{B}) \mathbf{B}}{|B^2 \mathbf{A} - (\mathbf{A} \cdot \mathbf{B}) \mathbf{B}|} C. \quad (5)$$

We now wish to highlight regions where this scalar field F is high along a thin filament parallel to the magnetic field. We do by looking at the second spatial derivatives perpendicular to the magnetic field:

$$G = -r^2 \mathbf{r} \cdot \hat{\mathbf{C}} (\nabla \times \mathbf{B})^4 ((\mathbf{m} \cdot \nabla)^2 F + (\mathbf{n} \cdot \nabla)^2 F) \quad (6)$$

where \mathbf{m} and \mathbf{n} are unit vectors perpendicular to both \mathbf{B} and each other. Adding the current density and radius factors both help to make the path of the torus stand out better. It is this scalar field G which is plotted in the smaller frames of Fig. 20.

In addition to these plots, it is possible to project the surface of the star into two dimensions. Enjoying the luxury of being subject to neither navigational nor political considerations, we picked the simplest projection imaginable, that is, longitude becomes the x coordinate and latitude becomes the y coordinate. This is useful in particular when the field has a dominant component by which an axis can be defined. In many of the configurations evolving found here, a dipole component dominates at the surface, and its axis (the axis \mathbf{M} defined in Eq. (3)) is then taken for the (x, y) -projection.

The shape and evolution of the magnetic field can be quantified in the following ways. Firstly, as the length of the intersection between the $B_r = 0$ and $r = R_*$ surfaces – plotted in the following section is W , the length of this intersection divided by $2\pi R_*$. A value of 1 is expected for a dipolar field; a value of five or more implies a field with structure on the scale of a few grid points.

Secondly, the surface value of B_r can be decomposed into spherical harmonics. This gives an indication of how well ordered the field is – if we plot the energy of the dipole, quadrupole, octupole and higher orders as a fraction of the total field energy, it is easy to see how ordered or chaotic the field is. The coefficients can also be compared directly to the results of observational studies which have assumed a dipole or dipole and quadrupolar field. The axis \mathbf{M} defined above is parallel to the dipole moment.

Thirdly, we can break up the magnetic field into its three components in spherical coordinates (again using the axis \mathbf{M}), and then calculate the total energy in the toroidal component and in the poloidal component.

Finally, we calculate a radius a_m to quantify the volume occupied by the magnetic field:

$$a_m^2 = \frac{\int B^2 r^2 dV}{\int B^2 dV}. \quad (7)$$

This is especially useful for calculations of the longer-term diffusive evolution of the field, giving a measure how far outwards the field has spread from its initial form. The initial value of a_m is roughly equal to the length scale r_m of the initial field configuration (Sect. 5). It will also depend to some small extent on the exact form of the initial random field, in general $a_m(t = 0) \approx 0.9r_m$.

7. Results

As described in Sect. 3.1, relaxation of the magnetic field in the atmosphere is an integral part of the stability problem. As a first

test, however, a field was evolved in a star without atmosphere, at a resolution of 96^3 . This evolution would be typical of the evolution of a field at high β , buried inside the star.

After around 3 Alfvén crossing times (based on the initial field strength), the field energy has decayed by a factor of around 50 and has assumed a configuration which then appears to be stable. The poloidal component is very similar to that which would be produced by an azimuthal current loop near the equator of the star. The toroidal component then threads along this loop. The loop is generally a little off-centred both in radius and in latitude, and almost circular.

This field then gradually diffuses outwards into the atmosphere, maintaining its overall form as it does so, until of course it reaches the edges of the computational box and the periodic boundary conditions have an effect.

Several cases like this were run, (also at resolution 96^3), with different realisations of the random initial field. The outcome was always similar – in all cases a twisted torus field was produced, either right or left-handed. In a small proportion of cases, both right and left-handed tori were formed above one another, in which case one eventually dies away.

This suggests an important first conclusion: there is perhaps only one possible type of stable field configuration in a star. If others exist, they are apparently not easily reached from random initial conditions.

Next, we consider cases where the magnetic field is allowed to relax to a potential field in the atmosphere, by means of the atmospheric diffusion term described in Sect. 3.1. The initial evolution of the field is unaffected by the addition of the atmospheric diffusion term, provided that the length scale r_m of the initial field configuration (cf. Eq. (2)) is small enough. This comes of course as no surprise, since the properties of the atmosphere should have no effect on a field confined to the stellar interior. Fig. 6 shows, in a sequence of snapshots, the early evolution of the field, from the initial random state into the torus shape. For this run, a resolution of 144 cubed was used – higher than for the other runs, since a duration of just a few Alfvén-crossing-times was required. The torus field forms on a timescale of the order of a few Alfvén crossing times, which is equal to around 0.6 days at this field strength. The snapshots in the figure are taken at times $t = 0, 0.18, 0.54$ and 5.4 days, i.e. after 0, 0.3, 0.9 and 9 Alfvén crossing times. Once the torus is clearly defined, it makes sense to talk about toroidal (azimuthal) and poloidal (meridional) components of the field, by defining them relative to the axis of the torus. The axis definition M (cf. Eq. (3)) was used for division into toroidal and poloidal components.

By the time the torus field has formed, the field energy has decayed by a factor of 50 or so. As the field then diffuses gradually outwards, the effect of the atmospheric diffusion term begins to show itself. This is because at first, the field is confined to the interior and consequently unaffected by the properties of the atmosphere. Once the field has diffused outwards somewhat it will clearly begin to be affected by the fact that the star has a surface beyond which the properties of the material are different.

To illustrate this Fig. 7 shows the energy in the poloidal field component, as a fraction of the total magnetic energy (de-

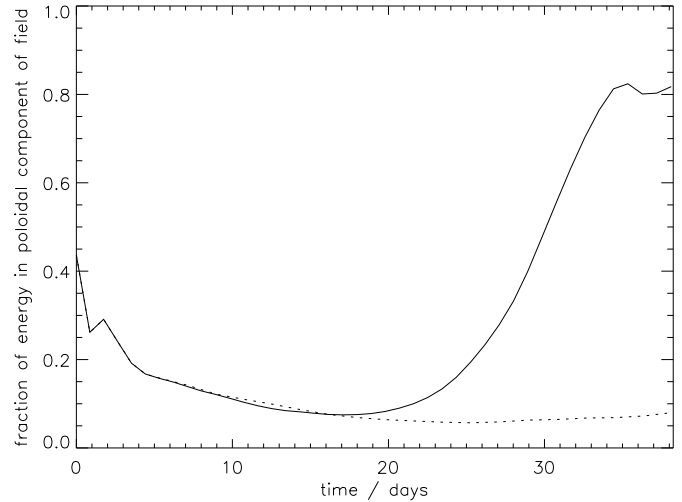


Fig. 7. The fraction of the magnetic energy contained in the poloidal field for the two runs (at resolution 96^3) with the atmospheric diffusion term switched on (solid line) and off (dotted line).

scribed in Sect. 6). It is seen that the atmospheric diffusion term causes the poloidal component of the field to become stronger than the toroidal. When it is first formed, the torus field has something like 90% of its energy in the toroidal component, but a non-conducting atmosphere cannot of course support a twisted field outside of the star. Only the poloidal component survives the move from inside to outside. The energy of the toroidal component therefore falls compared to that of the poloidal component.

It is useful to check that this diffusion term is doing its job properly, i.e. to suppress the electric current in the atmosphere. To this end, we can look at the current density in the stellar interior compared to that in the atmosphere. In Fig. 8 we have plotted the radial averages of the field strength and of the current density (multiplied by the stellar radius R_* to give the same units as field strength), at times $t = 5.4$ and $t = 27.2$ days, i.e. during the slow outwards diffusive phase of the field’s evolution. It is the difference between these two quantities that we are interested in, and we can see that when the diffusion term is switched on, the field in the atmosphere is stronger than when it is switched off – this is because a potential field, which is what we have when the term is switched on, responds immediately to the field on the stellar surface, while a field takes much longer to penetrate a current-carrying atmosphere. Also, the diffusion term has the effect of reducing by a factor of ten or so the value of $R_*|\mathbf{I}|$ in relation to the field strength. All subsequent discussion is limited to runs performed with the atmospheric diffusion term switched on.

In Fig. 11, we can see how the torus changes as it diffuses outwards. At two times ($t = 22.6$ and 31.9 days) field lines are plotted – it is clear that at the time of the first snapshot, the field is mainly toroidal, but then the poloidal component grows in relation to the toroidal.

As the field diffuses further outwards, the shape of the field changes. The torus starts distorting as if it were a loaded spring trapped inside a hollow ball – it changes first from a circular

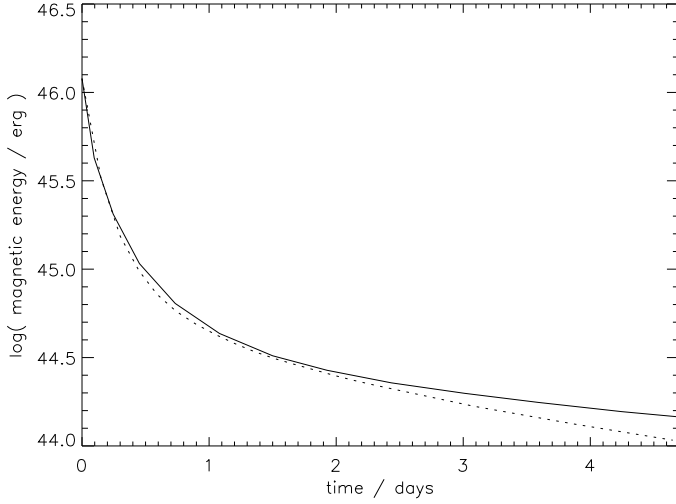


Fig. 9. Test of the field amplitude rescaling scheme: The magnetic energy $E(t)$ is plotted against the time t , with rescaling (solid line) and without (dotted line).

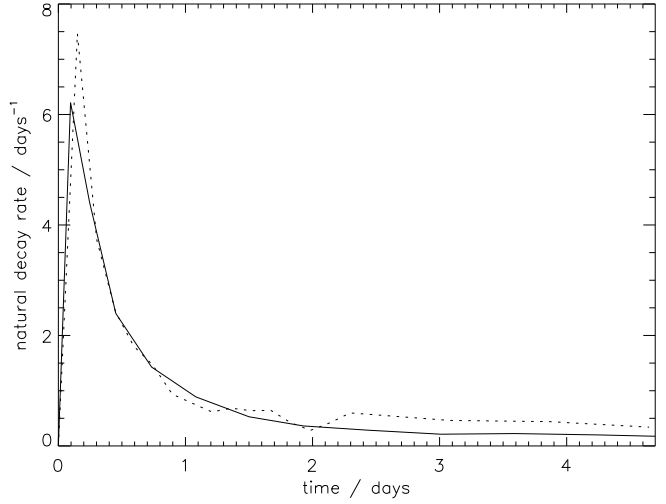


Fig. 10. As Fig. 9, but showing the field decay rate \dot{E}/E .

shape to the shape of the line on the surface of a tennis ball, and then to an more contorted shape, as shown in Fig. 20.

7.1. Tests

The validity and accuracy of the code can be judged from the set of results to be published in Braithwaite (2005). In these calculations, a series of stability calculations for toroidal field configurations in stably stratified stars are reported and compared with known analytical results. The good agreement found there demonstrates the applicability for problems like the present stellar MHD problem.

As described in Sect. 3.3, a *rescaling* procedure is used to increase the speed of the calculation. Since this procedure can be formally justified only in the limit $\eta/R \ll v_A \ll c_s$, tests were done comparing the evolution of a given initial field with and without this procedure. The result of such a test is shown in Figs. 9 and 10. Plotted, for both runs, are the total magnetic energy as a function of time and its decay rate. The figures show that the rescaling scheme reproduces field decay properly, at least when the field’s evolution is primarily on the dynamic time scale and not Ohmic. Once the stable field has appeared and diffusive processes become important, the scheme ceases to speed up the evolution. This manifests itself in the two figures in a divergence of the two runs at later times: the process becomes less accurate when diffusive processes take over from dynamic evolution.

Fig. 12 compares the end result of the evolution of the field in the two cases at time of $t = 4.5$ days. This shows the level of difference introduced in the field configuration by the rescaling process.

7.2. The characteristic size of the initial field configuration

The evolution is found to depend on the initial state of the magnetic field, or at least, on the initial length scale r_m (cf. Eq.

(2)) of the field. For small r_m , the field configuration is concentrated more towards the centre of the star. Runs were done with different values of r_m but with the same total magnetic energy. The field finds the torus configuration only if r_m is below a certain value, so that if r_m is smaller than this value, the torus produced diffuses gradually outwards until at some point it starts the ‘tennis ball’ distortion described above. The smaller r_m is, the smaller the torus produced is, and the longer this diffusive phase lasts. If r_m is above the critical value, the field goes straight into the distorted state without ever reaching the regular torus shape. So its value has no effect on the final state of the field, i.e. one of fast decay caused by dynamic instability. In the runs described above, we used $r_m = 0.25R_*$. To look at the effect of r_m , we did otherwise identical runs at resolution 72^3 with $r_m = 0.14R_*$, $0.25R_*$, $0.39R_*$ and $0.57R_*$. These runs can be compared by looking at the poloidal field energy as a proportion of the total energy – see Fig. 13. It can be seen that the value of r_m affects the route taken to reach the final state, but has no effect on the final state itself. The run with $r_m = 0.57R_*$ never reaches any stable state at all; the other three runs with smaller r_m do reach it, and stay in it longer the smaller r_m is.

This can be confirmed by looking at the rate of decay of the field, as plotted in Fig. 14. It can be seen that the greater r_m , the sooner the point is reached at which the field begins to decay quickly.

7.3. A quantitative look at the diffusive phase of evolution

Once the stable torus field has formed, it gradually diffuses outwards. If the configuration was initially concentrated towards the centre, it is then possible that the strength of the field on the surface increases, despite the fact that the total magnetic energy goes down.

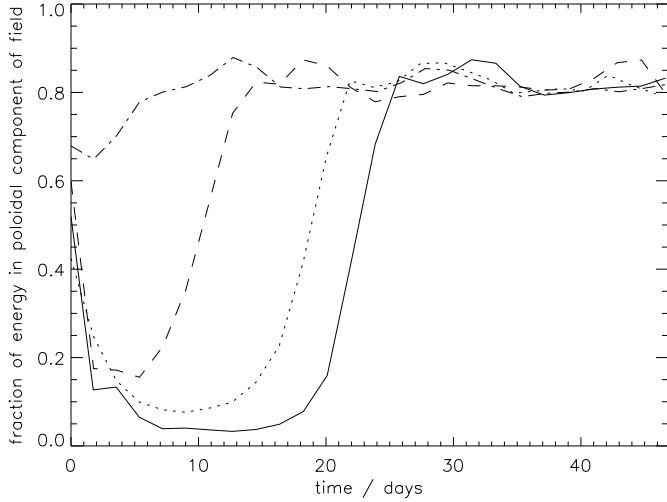


Fig. 13. The effect of the length scale of the initial field configuration on the evolution of the field. The poloidal fraction of the magnetic energy is plotted for $r_m = 0.14R_*$ (solid line), $0.25R_*$ (dotted), $0.39R_*$ (dashed) and $0.57R_*$ (dot-dashed). It can be seen that the initial conditions merely determine the route taken to the final state, not the final state itself.

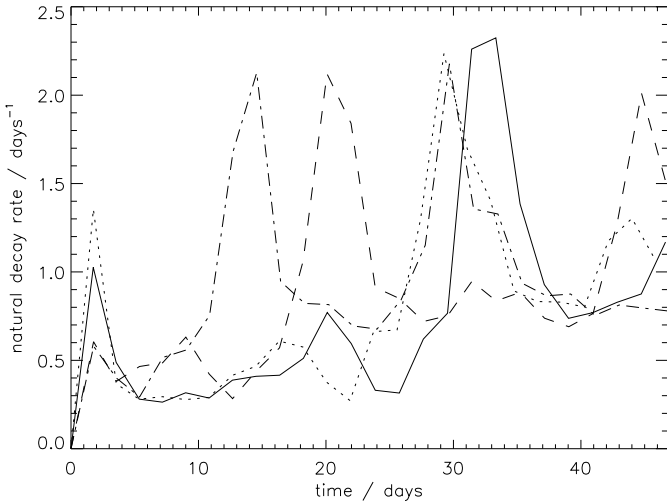


Fig. 14. The rate of decay of the field, for the four runs with different values of r_m .

To look at this in a quantitative manner, we have introduced a diffusivity with the functional form of the Spitzer’s (1962) conductivity for ionised plasmas, applicable in stellar interiors:

$$\eta_0 = KT^{-3/2}. \quad (8)$$

Here $K \approx 7 \times 10^{11} \ln \Lambda$ where the Coulomb logarithm $\ln \Lambda$ is of order 10 in a stellar interior.

Adding this diffusivity to the code would result in the field evolving much too slowly to be computationally practical. We can make use of the fact that, in the stage we are interested in here, the field is evolving on the diffusive time-scale. In this case, an increase of the diffusivity by a constant factor, while maintaining the functional dependence (8), is equivalent to a decrease in the time-scale of evolution. Thus, we use a diffusivity of the form (8), with K adjusted to yield a speed of evo-

lution that is sufficiently long compared with the Alfvén time-scale, but still short enough to be computationally feasible. The evolution can then be scaled afterwards to a realistic time axis.

As the initial conditions, we used the output from the fiducial run at resolution 96^3 at a time $t = 4.4$ days – once the stable torus field has formed. The numerical diffusion scheme, which is required to hold the code stable when the field is evolving on a dynamic time-scale, was switched off for these runs. The field rescaling routine (Sect. 3.3) was also switched off. We ran the code with η/η_0 equal to 10^{11} , 1.7×10^{11} , 3×10^{11} , 5.5×10^{11} , 10^{12} , 1.7×10^{12} and 3×10^{12} .

We are interested in what happens to the field strength on the surface of the star during this phase of evolution, since only the surface field is observed. Fig. 15 is a plot of this surface field (to be precise, the root-mean-square of its modulus) as a function of time, for the runs with different values of η/η_0 . The field strength is indeed found to increase; the higher the diffusivity, the faster the surface field grows.

Looking at the result of Hubrig et al. 2000a, which suggests that Ap stars typically become visibly magnetic after 30% of their main-sequence lifetime (which works out at around 3×10^8 years), it would be interesting to see how quickly the surface field in these runs is rising. We can obtain a time-scale if we divide the field strength by its time derivative. If we do this for the $\eta/\eta_0 = 10^{12}$ case, we obtain the time-scale 0.8 days; we can therefore infer that if we set $\eta = \eta_0$, we would measure a timescale 2×10^9 years. This is somewhat larger than the main sequence lifespan, but still within an order of magnitude.

We conclude that Ohmic diffusion of an internal magnetic field is a plausible model for the increase of the surface magnetic field with time implied by the observations of Hubrig et al. Quantitative improvements in the physics used (stellar structure model, precise value of η) and numerical resolution will be needed, however, to test this idea more securely.

It is useful to check that the time-scale really is dependent on the diffusivity in the way we have assumed, i.e. that the two are inversely proportional. To this end, we have plotted the reciprocal of the timescale measured as a function of η/η_0 in Fig. 16. The two are found to be proportional to each other, except at the two ends of the range where other numerical effects come into play.

7.4. Change in the surface field shape during the diffusive phase

We have seen in the last section that the strength of the field on the surface of the star goes up during the diffusive phase of evolution, after the stable torus field has formed in the interior. However, this is not the only change visible to an outside observer – the *shape* of the surface field also changes. Immediately after the stable field configuration has been reached in the interior, the field in the outer part of the star has yet to relax to a dipolar shape; which does then gradually happen, but only on the longer Ohmic time-scale. This implies that a field configuration consisting of a regular torus

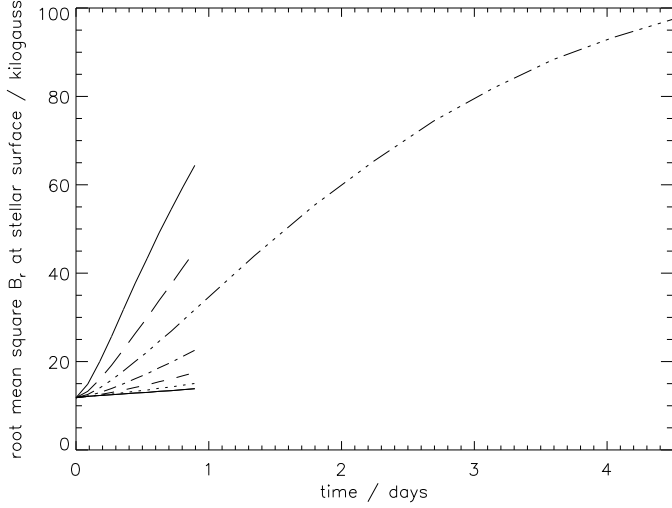


Fig. 15. Root-mean-square B_r at the surface of the star, as a function of time. Seven values of diffusion: $10^{11}\eta_0$ (solid), $1.7 \times 10^{11}\eta_0$ (dotted), $3 \times 10^{11}\eta_0$ (dashed), $5.5 \times 10^{11}\eta_0$ (dot-dashed), $10^{12}\eta_0$ (dot-dot-dot-dashed), $1.7 \times 10^{12}\eta_0$ (long-dashed) and $3 \times 10^{12}\eta_0$ (solid). The higher the diffusion, the faster the field on the stellar surface increases.

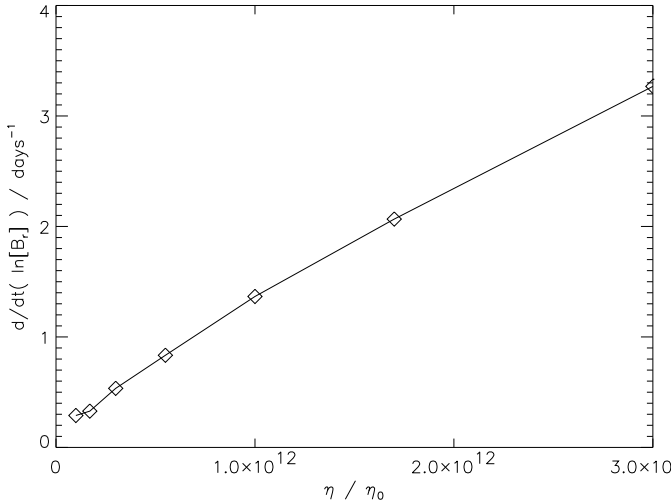


Fig. 16. The reciprocal of the time-scale on which the surface field is increasing, $\bar{B}_r / \partial_t \bar{B}_r$, as a function of η / η_0 .

field in the centre of the star and an irregular field in the outer part can be dynamically stable.

To illustrate this, it is first helpful to look back at Figs. 10 and 9, in which we can see that the stable field configuration has formed within one day or so, i.e. on the order of the Alfvén crossing-time, and that after that the field evolves by mainly diffusive processes, on an Ohmic time-scale.

Fig. 17 is a projection onto two dimensions of the field’s radial component B_r on the stellar surface. This is plotted at four points in time, the first being $t = 0$, the second just after the stable field has formed at $t = 2.6$ days, and the third and fourth at $t = 9.8$ and 22.6 days respectively. It is easy to see how the field on the surface approaches a dipole.

This can also be looked at in a more quantitative manner. To this end, we need to find a way to define a length scale on the

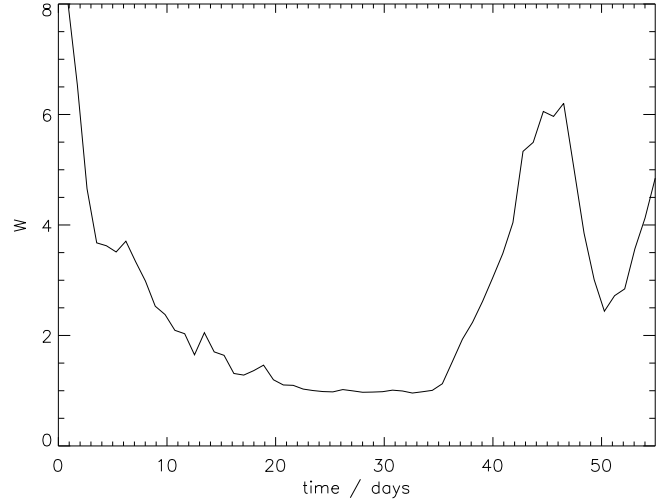


Fig. 18. W , plotted above, is defined as the length of the line separating positive from negative B_r on the surface of the star, divided by $2\pi R_*$. During the diffusive phase, this has its dipole value of unity; when the field becomes unstable it grows.

stellar surface – we use the quantity W defined in Sect. 6 as the total length of the line(s) on the surface of the star which separate(s) regions of positive and negative B_r , divided by $2\pi R_*$. (We may then expect that the typical length scale \mathcal{L} is given by the area of the surface of the star divided by the length of this $B_r = 0$ line, so that $\mathcal{L} \sim 2R_*/W$.) The quantity W in the fiducial run at resolution 96 is plotted in Fig. 18. It begins large, slowly falls to its minimum value (of unity) as the field in the outer part of the star relaxes to a regular dipolar shape and as the torus field diffuses outwards, and then (as described in the next section) suddenly grows.

It is also interesting to look at the decomposition into spherical harmonics of B_r on the stellar surface. The proportions of energy in each spherical harmonic order is plotted in Fig. 19. When the stable torus field has just formed, most of the energy is in the higher-order components, and as the field gradually diffuses outwards, almost all of the energy goes into the dipole component, with the quadrupolar component making up almost all of the rest (remember that an offset dipole can be expressed as dipole plus quadrupole). At $t = 22.6$ days, corresponding to the last frame of Fig. 17, virtually no energy is present in the octupole or higher orders. As described in the next section, the field then later becomes unstable, and the energy goes back into the higher components.

From this, it is possible to make a hypothesis: that Ap stars with near-exact dipolar fields are likely to be older than Ap stars with more structure on smaller scales. However, there will be factors other than age which we would expect to determine how dipole-like the surface field is, for instance, the degree to which the field was concentrated into the centre of the star at the time of formation – a highly concentrated initial field would result, after formation of the stable torus field, in a field at the surface with significant higher-order components. The relative importance of these factors is uncertain.

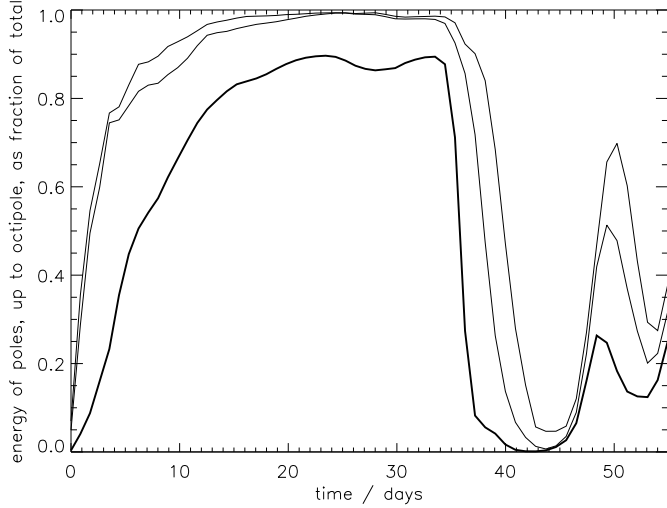


Fig. 19. The energy of the B_r component on the surface of the star, broken down into its dipolar, quadrupolar, octupolar and higher components, as proportions of the total energy. The dipolar energy is represented by the space between the x axis and the thick line, the quadrupolar energy is represented by the space between the thick line and the one above it, etc. The transition from stable to unstable at $t \approx 35$ days can be seen, as the dipole component suddenly loses its energy and the surface field becomes dominated by higher components, first by quadrupole and octupole, then by even higher orders.

7.5. The final, unstable phase of evolution

As mentioned above, when the stable torus field diffuses outwards to a certain radius, it eventually becomes unstable and decays. The shape of the field changes from an ordered, large-scale shape to a disordered, small-scale shape which then constantly changes and moves around. This fall of length scale brings about an increase in the rate at which energy is lost via Ohmic diffusion, since the time-scale over which the latter occurs is proportional to the square of the length scale.

Fig. 20 shows the evolution of this final instability, from the moment when it begins to a time when the length scale has fallen significantly. Fig. 21 is a projection onto two dimensions of the field's radial component B_r on the stellar surface. The axis \mathbf{M} at the time of the third picture ($t = 31.9$ days) is used for the projection, although this axis moves by less than five degrees between then and the time of the last picture in the sequence. The third, fourth, fifth and sixth frames in Fig. 21 correspond to the four frames in Fig. 20.

To see the length scale falling, we can use the quantity W , which was plotted in Fig. 18. At around $t = 35$ days, W suddenly rises, and since the length scale is given by $\mathcal{L} \sim 2R_*/W$, i.e. the length scale is inversely proportional to W , this means the length scale is going down.

As we saw in Fig. 19 (which shows how the energy of the field on the surface is divided up between the different components in spherical harmonics), the field is almost entirely dipolar just before the field becomes unstable. Then, the dipolar component decays very rapidly and higher orders take over.

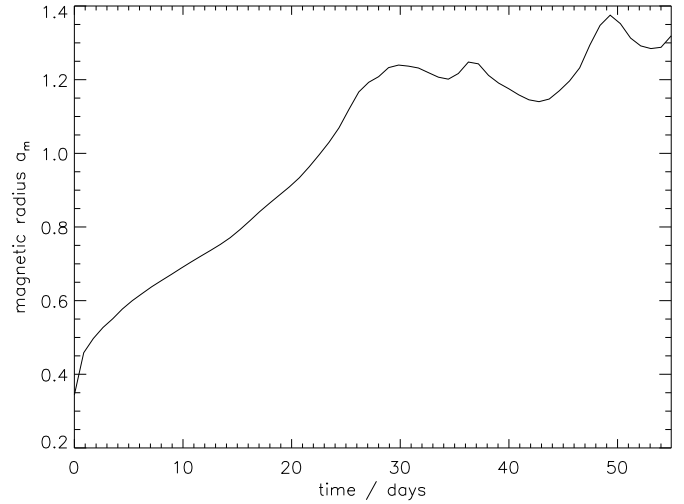


Fig. 22. The magnetic radius a_m against time. It can be seen that during the diffusive phase, the field moves slowly outwards, and that the field enters the unstable phase only once this outwards diffusion has ended. This transition to instability, as can be seen for instance in Fig. 19, occurs at $t \approx 35$ days.

The beginning of this unstable phase marks the end of the gradual outwards diffusion of the field. This can be seen by looking at the value of the magnetic radius a_m (defined in Eq. (7)), as plotted in Fig. 22.

8. Comparison with observations

The main result of this study is the existence of a dynamically stable field which can survive for a long time, and assuming the validity of the diffusivity extrapolation described in Sect. 7.3 and Fig. 16, at least as long as an A-star main sequence lifetime. At the surface of the star, this field is found to be mainly dipolar, with smaller contributions from quadrupole and higher components. This is largely in agreement with the observations described in Sect. 1.1; it is observed that the field on the surface of Ap stars is ordered on a large scale and mainly dipole in form.

We should like to make this comparison between the result of this study and the observations in a slightly more quantitative manner. To this end we can calculate from the results found here some quantities which can be directly observed. This bypasses the processes involved in reconstructing the surface field from observations.

The most common method for looking at the magnetic field of a star is the analysis of the Stokes I and V profiles and of frequency-integrated Stokes Q and U profiles. This can yield various quantities depending on factors such as the rotation velocity of the star (which broadens the spectral lines and therefore makes the analysis more difficult). The most easily obtained of these quantities are the *longitudinal field* B_l and the *field modulus* B_s , which are obtained from weighted averages over the visible hemisphere of the line-of-sight component $\langle B_z \rangle$ and of the modulus $\langle B \rangle$ of the field respectively. They are weighted with the function $Q(\Theta)$, where Θ is the angle be-

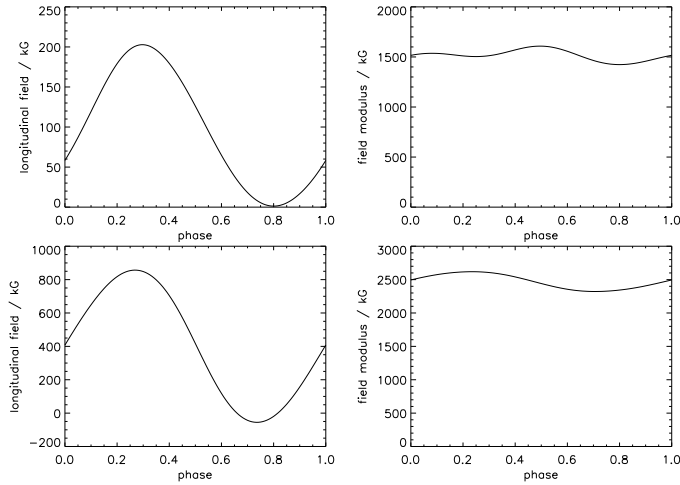


Fig. 23. Longitudinal field and field modulus at two stages during the field’s evolution, as seen over one rotation. Upper left frame: longitudinal field at $t = 22.6$ days; upper right: field modulus at $t = 22.6$ days; lower left: longitudinal field at $t = 31.9$ days, lower right: field modulus at $t = 31.9$ days

tween the normal to the stellar surface and line of sight, which is given by (Landstreet & Mathys 2000)

$$Q(\Theta) = [1 - \epsilon_c(1 - \cos \Theta)][1 - \epsilon_l(1 - \cos \Theta)], \quad (9)$$

where ϵ_c and ϵ_l are limb darkening and line weighting coefficients, given the values 0.4 and 0.5.

As the star rotates, these quantities B_l and B_s change; we can calculate them as a function of rotational phase. We just need to choose a rotational axis, and an angle i between this rotational axis and the line of sight. The matter of whether the magnetic and rotation axes are likely to be close together or far apart is a little uncertain. It is possible that rotation has a direct effect on the direction of the magnetic axis, or that the magnetic field makes the rotation axis precess and migrate (Mestel & Takhar 1972 and references therein) – whether this tends to increase or decrease the angle between the two depends on the shape of the field. For the slow rotators though, it seems that the two are close together (Landstreet & Mathys 2000), so we shall pick an angle 30° . For i , we choose the median value (the distribution is of course random) of 60° .

We calculate the longitudinal field and field modulus from the fiducial run described in Sect. 7. We have done this at two points in time while the stable torus field is present, $t = 22.6$ and 31.9 days (corresponding to the second and third frames of Fig. 21), the surface field being significantly stronger at the later time. These quantities are plotted, as a function of rotational phase, in Fig. 23.

At the later of these two times, both the longitudinal field and the field modulus are variable in a sinusoidal fashion, which is what is observed in most Ap stars. At the earlier time $t = 22.6$ days, the variation is not purely sinusoidal. This behaviour has been observed for instance in the slowly rotating Ap star HD 187474 (Khalack et al. 2003).

9. Discussion and conclusions

We have modelled an Ap star and evolved its magnetic field in time using numerical MHD, starting with a random field configuration in the interior of the star. Any random field configuration is in general unstable and will decay on a timescale comparable to the time taken by an Alfvén wave to cross the star; this is indeed exactly what happens in these simulations. The field evolves into a stable ‘twisted torus’ configuration, which is then stable on an Alfvén time-scale (dynamic stability).

The configurations found were always of the same kind: a nearly axisymmetric torus inside the star, with toroidal (azimuthal) and poloidal (meridional) components of comparable strength. Depending on the particular random field present at the beginning, the torus which emerges is either right or left handed, and is in general a little displaced from the centre of the star. This torus forms the stable core of the configuration. Wrapped around it are poloidal field lines that extend through the atmosphere. These field lines cause the surface field to form an approximate dipole, with smaller contributions from higher multipoles.

The first conclusion to be drawn from this study is therefore the probable existence of stable field configurations in stably stratified stars. Our results provide the first plausible field configurations that explain both the stability and the surface appearance of A-star fields. We consider the results to be strong evidence in favour of the ‘fossil field’ model for Ap stars.

The second main result concerns the secular evolution of the stable field configurations. By Ohmic dissipation the field diffuses slowly outwards, while maintaining its overall shape. In the process, the strength of the field on the surface *increases* and the topology of the field in the interior undergoes a gradual change, from mainly toroidal to mainly poloidal. To understand why this happens, one first needs to understand that the toroidal field can only thread through those poloidal field loops which are closed inside the star. If toroidal field were present in regions where the poloidal field lines go all the way through the star and close outside, the field lines would be in effect entering the star at the north pole, twisting around inside the star, and exiting at the south pole. Due to the rapid relaxation of the atmospheric field, this twist is removed almost instantaneously, such that the toroidal field component is always small outside the star. As a result, the field line does not support a torque any more, and the interior part of the field line unwinds on an Alfvén time-scale (by azimuthal displacements) until only its poloidal component remains. This is sketched in Fig. 24. As seen in a projection on a meridional plane, the toroidal field component is restricted to those field lines that are closed within the star. As these closed field lines diffuse to the surface, their toroidal component is released, increasing the ratio of poloidal to toroidal field energy.

At some point, when the torus of closed field lines is close to the surface of the star, the (relative) increase of the poloidal field causes the torus to lose its circular shape. Its core, now located just below the surface, twists out of the plane. At first, this twist is like the seams on a tennis ball and thereafter becomes increasingly complicated. This continues until the diffusive timescale \mathcal{L}^2/η falls to the Alfvén time-scale. The field

then decays on an extremely short timescale compared to the lifetime of the star.

The diffusive evolution of the field thus agrees with the observational result in Sect. 1.1 of Hubrig et al. (2000a), that Ap stars are typically more than 30% of the way through their main-sequence life. The time-scale for this increase is found to be around 2×10^9 years, somewhat longer than 30% of the main-sequence lifetime of an A star (30% of 10^9 years), but it should be stressed that any accurate determination of this diffusive time-scale would have to use a more accurate modelling of the stellar structure and the magnetic diffusivity than that employed here.

For our results to hold as an explanation of A-star magnetic fields, the stars must, at the time of their formation, have contained a strong field. This initial field can be of arbitrary configuration, except that it must have a finite magnetic helicity and must be confined mainly to the core. Why only some A stars show a strong field is another question. There is of course the obvious possibility that the $\sim 90\%$ of A stars not observed to be magnetic simply contained, for whatever reason, no strong field at birth. There are however two other possible reasons, albeit also with no obvious explanation for the birth state required. Firstly, it is possible that most A stars are born with a strong field which is not sufficiently concentrated into the core, so that it quickly or immediately becomes unstable and decays, analogous to the run with $r_m = 0.57R_*$ described in Sect. 7.2 and Figs. 13 and 14. Secondly, the field in most A stars could be more concentrated towards the centre than in Ap stars, so that it does not have time to manifest itself at the surface during the main sequence.

It may seem unnatural that a newly born star should have its magnetic field concentrated into the core. However, this may be a logical consequence of flux conservation during formation (see, for instance, Mestel & Spitzer 1956, Mestel 1966). Assuming that the field in the progenitor cloud is of uniform strength, and that the topology of the field does not change, the field strength in the newly formed star will be proportional to $\rho^{2/3}$. In a polytrope of index 3, as we have used for this model, the ratio of thermal to magnetic energy densities $\beta = 8\pi e\rho/B^2$ will be constant, independent of radius. This is roughly the situation we have in the fiducial run in this study with $r_m = 0.25R_*$ (see Fig. 4), and that is indeed sufficiently concentrated to produce a stable torus field. This is assuming that the field the main-sequence star is born with comes directly from the cloud it formed from. There is of course another possibility: that of a dynamo in the pre-MS star which uses the cloud field merely as a seed. The magnetic field energy in this case is however also likely to be concentrated where the density is highest, i.e. in the centre.

There are examples of binary systems containing both a magnetic A star and a non-magnetic A star. This rules out chemical composition (*overall* chemical composition, not the composition we see on the surface, which is the result itself of the magnetic field) as the reason for the difference. It perhaps also rules out the field strength in the cloud from which the star condenses. It does not rule out the initial angular momentum distribution, and the effect this may have on any kind of dynamo driven by differential rotation; indeed it is possible that

rotation has an effect on whether the field emerges to be seen at the surface (Mestel & Moss 1977). Nor does it rule out differences in the precise shape of the field in the accretion discs that feed the growing protostar. Some fields of random shape will find their way to the stable configuration faster than others, losing less magnetic flux in the process. This may also have an effect on the size of the torus produced, which may then, as described in the previous paragraph, determine whether any field is observed on the surface.

References

- Acheson, D.J., 1978, *Phil. Trans. Roy. Soc. Lond.*, A289, 459.
 Babcock, H.W., 1947, *Astrophys. J.*, 105, 105.
 Bagnulo, S., Landi Degl'Innocenti, M., Landolfi, M. and Mathys, G., 2002, *A&A*, 394, 1023.
 Belopolsky, A., 1913, *Astron. Nach.*, 196, 1.
 Bonazzola, S., Gourgoulhon, E., Salgado, M. and Marck, J. A., 1993, *A&A*, 278, 421.
 Bonsack, W.K. and Wolff, S.C., 1980, *AJ*, 85, 599.
 Borra, E.F., Landstreet, J.D. and Mestel, L., 1982, *Ann. Rev. Astr. Astrophys.*, 20, 191.
 Braithwaite, J., 2005, in preparation.
 Braithwaite, J. and Spruit, H.C., 2004, *Nature*, 431, 891.
 Chandrasekhar, S., 1961, "Hydrodynamic and hydromagnetic stability", Oxford Univ. Press.
 Cowling, T.G., 1945, *MNRAS*, 105, 166.
 Cowling, T.G., 1958, *IAUS*, 6, 105C.
 Deutsch, A.J., 1947, *Astrophys. J.*, 105, 283.
 Flowers, E. and Ruderman, M.A., 1977, *ApJ*, 215, 302.
 Gerth, E., Glagolevskij, Yu.V. and Sholz, G., 1997, in *Stellar magnetic fields*, ed. Yu.V.Glagolevskij and I.I.Romanyuk (Moscow), 67.
 Guthnick, P. and Prager, R., 1914, *Veröff. K. Sternw. Berlin Babelsberg*, 1, 1.
 Hubrig, S., North, P. and Mathys, G., 2000a, *ApJ*, 539, 352.
 Hubrig, S., North, P. and Medici, A., 2000b, *A&A*, 359, 306.
 Hyman, J., 1979, in R. Vichnevetsky, R.S. Stepleman (eds.), *Adv. in Comp. Meth. for PDEs - III*, 313.
 IRIS Explorer, <http://www.nag.co.uk>
 Khalack, V.R., Zverko, J. and Žižňovský, J., 2003, *A&A*, 403, 179.
 Kamchatnov, A.M., 1982, *Zh. Eksp. Teor. Fiz.*, 82, 117.
 Landstreet, J.D. and Mathys, G., 2000, *A&A*, 359, 213.
 Markey, P. and Tayler, R.J., 1973, *MNRAS*, 163, 77.
 Markey, P. and Tayler, R.J., 1974, *MNRAS*, 168, 505.
 Mathys, G., 1995a, *A&A*, 293, 733.
 Mathys, G., 1995b, *A&A*, 293, 746.
 Maury, A.C., 1897, *Harvard Ann.*, 28, 96.
 Mestel, L., 1966, *MNRAS*, 133, 265.
 Mestel, L. and Moss, D.L., 1977, *MNRAS*, 178, 27.
 Mestel, L. and Spitzer, L.Jr., 1956, *MNRAS*, 116, 503.
 Mestel, L. and Takhar, H.S., 1972, *MNRAS*, 156, 419.
 Morgan, W.W., 1933, *Astrophys. J.*, 77, 330.
 Nordlund, Å., Galsgaard, K., 1995, <http://www.astro.ku.dk/~aake/papers/95.ps.gz>
 North, P., 1993, in *IAU Colloq. 138, Peculiar versus normal phenomena in A-type and related stars*, ed. M.M.Dworetzky, F.Castelli & R.Faraggiana (ASP Conf. Ser. 44; San Francisco: ASP), 577.
 Piskunov, N. and Kochukhov, O., 2002, *A&A*, 381, 736.
 Pitts, E. and Tayler, R.J., 1986, *MNRAS*, 216, 139.
 Prendergast, K.H., 1956, *ApJ*, 123, 498.
 Roberts, P.H., 1967, "An introduction to magnetohydrodynamics", Longmans.

- Spitzer, L., 1962, "Physics of fully ionized gases", Interscience (John Wiley).
- Tayler, R.J., 1973, MNRAS, 161, 365.
- Wade, G.A., 1997, A&A, 325, 1063.
- Wright, G.A.E., 1973, MNRAS, 162, 339.

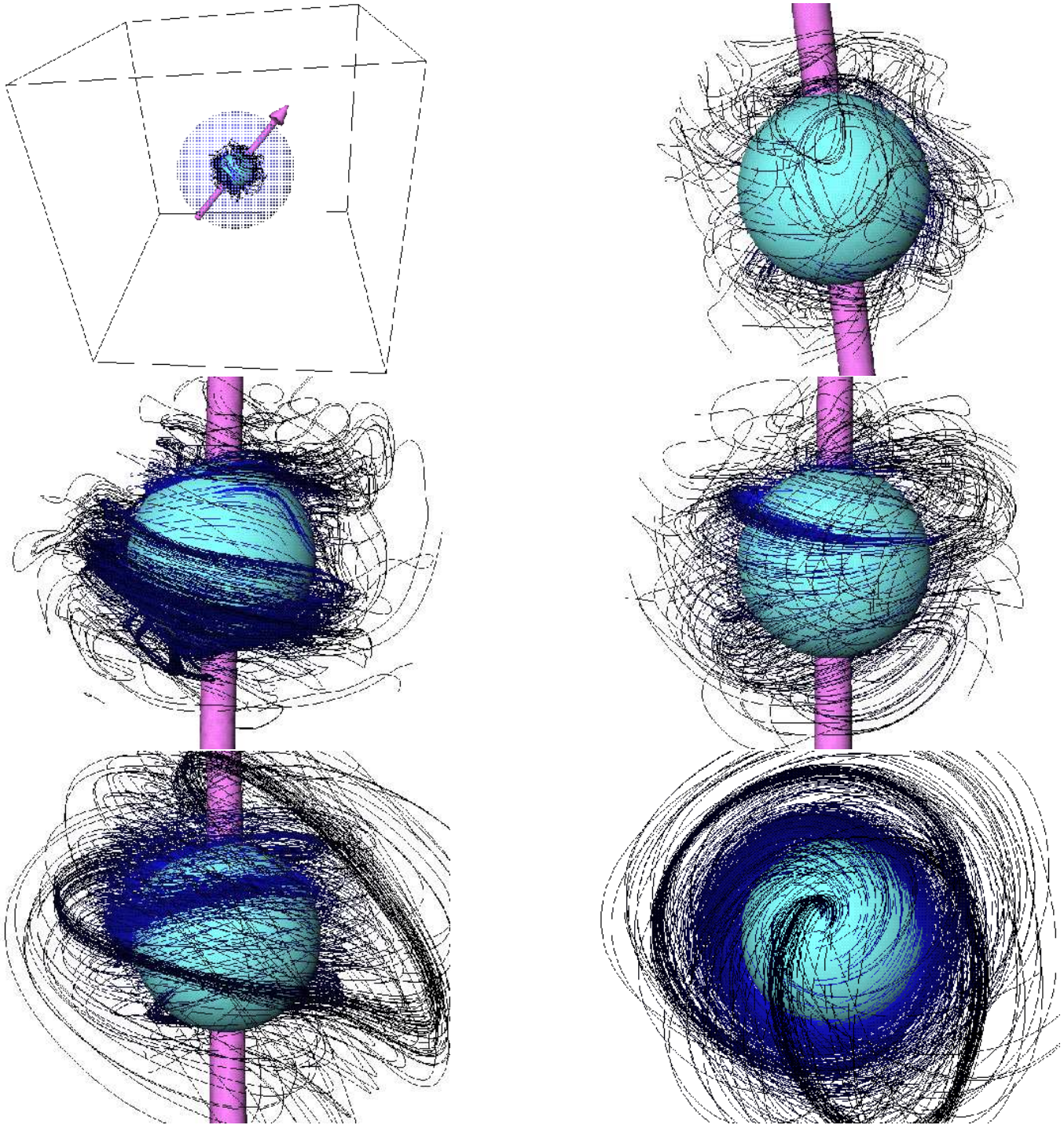


Fig. 6. The initial evolution of the field, plotted with IRIS Explorer. Plotted top left at $t = 0$ is the computational box, with field lines, the axis M and (only in this frame) the surface of the star. Also plotted in this frame, as in all of the frames, is a surface of constant radius ($r = 0.3R_*$), which helps to make it easier to see the field lines in the foreground. However, in this frame this is difficult to see. Therefore, the other frames are zoomed-in somewhat, so that only the $r = 0.3R_*$ surface is visible and not the surface of the star. Top right is also at $t = 0$, but viewed from a different angle, and zoomed-in. Middle left, middle right and bottom left are snapshots taken at times $t = 0.18, 0.54$ and 5.4 days. Bottom right is the last of these, looking down the magnetic axis.

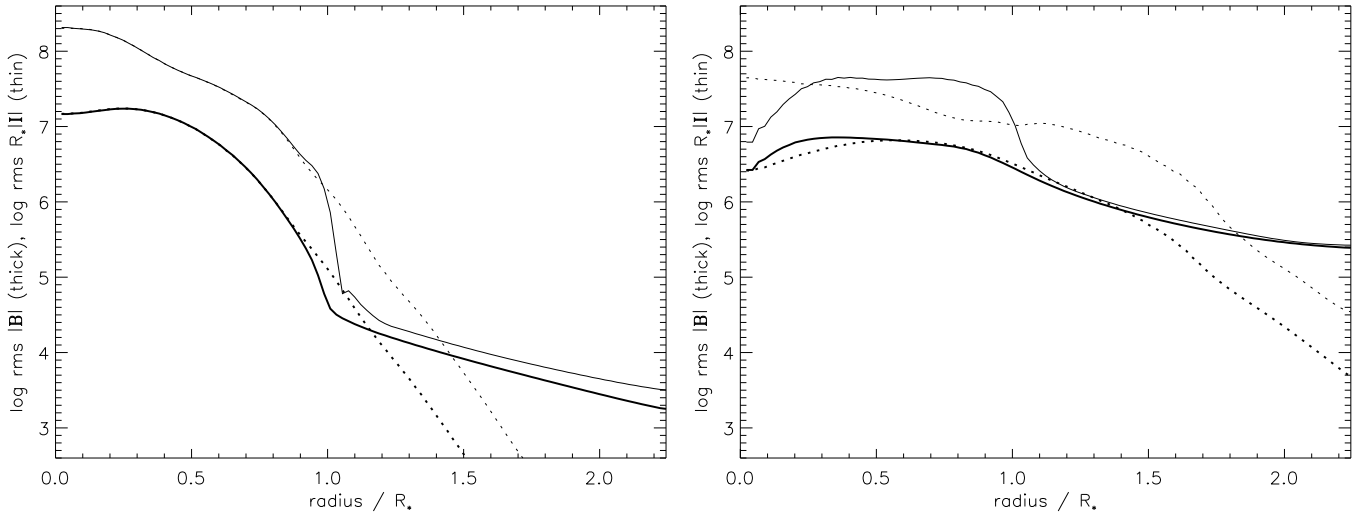


Fig. 8. Root-mean-square as a function of radius of field amplitude $|B|$ (thick lines) and current density $R_*|I|$ (multiplied by R_* out of consideration for units) (thin lines), for the two runs with the atmospheric diffusion term switched on (solid line) and off (dotted line), at times $t = 5.4$ (left) and $t = 38.1$ days (right).

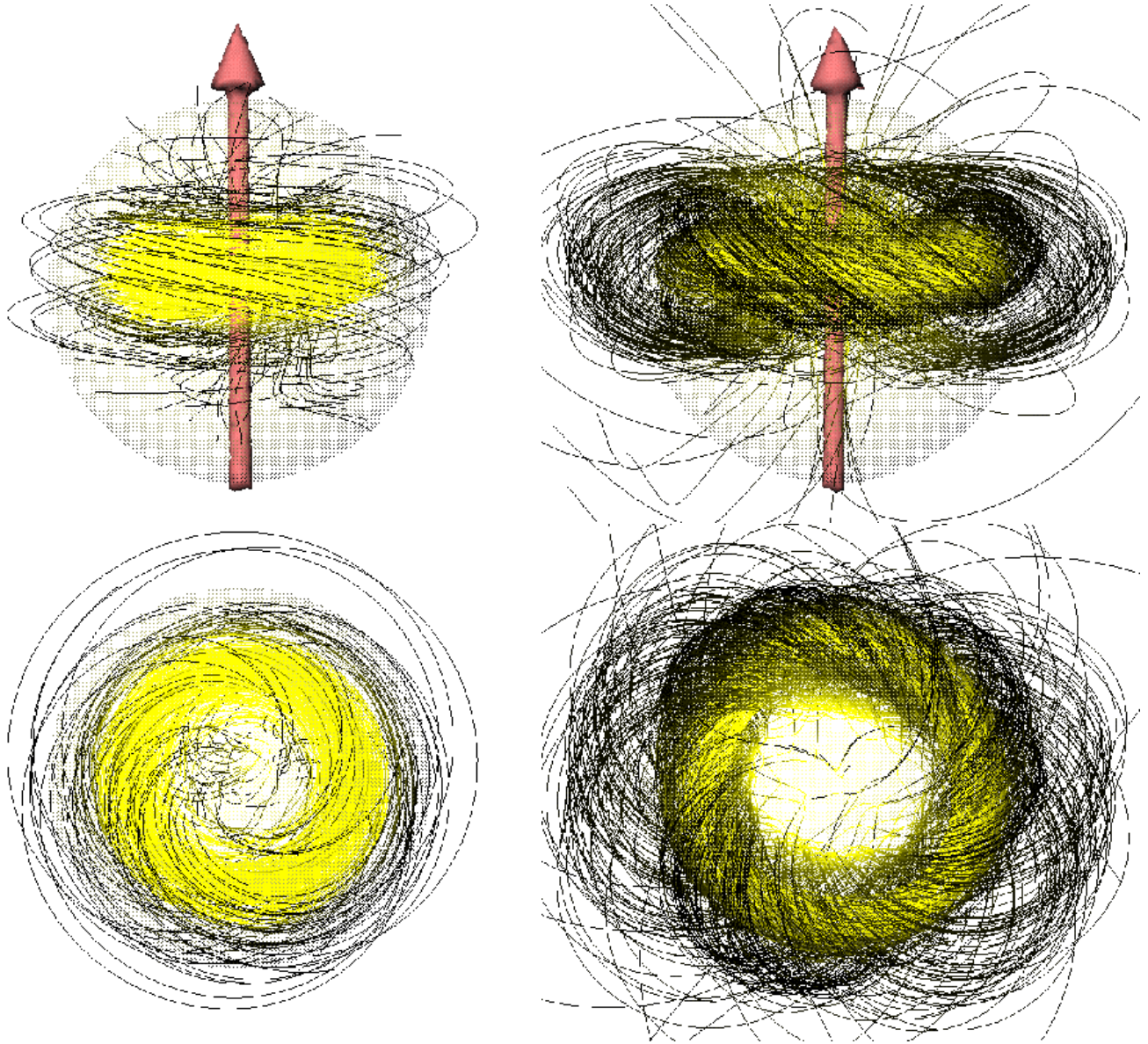


Fig. 11. Snapshots of the fiducial run at resolution 96^3 . Upper left, at $t = 22.6$ days, field lines are plotted, in addition to the magnetic axis M (the arrow) and a transparent sphere of radius R_* . Lower left, the same viewed from a different angle. Upper right and lower right, the same at a later time $t = 31.9$ days. As can be seen here as well as in Fig. 7, the proportion of energy in the poloidal field increases significantly between these two times, from 11% to 65%. This is caused by the outwards diffusion of the torus field – a greater proportion of the magnetic energy is in the atmosphere.

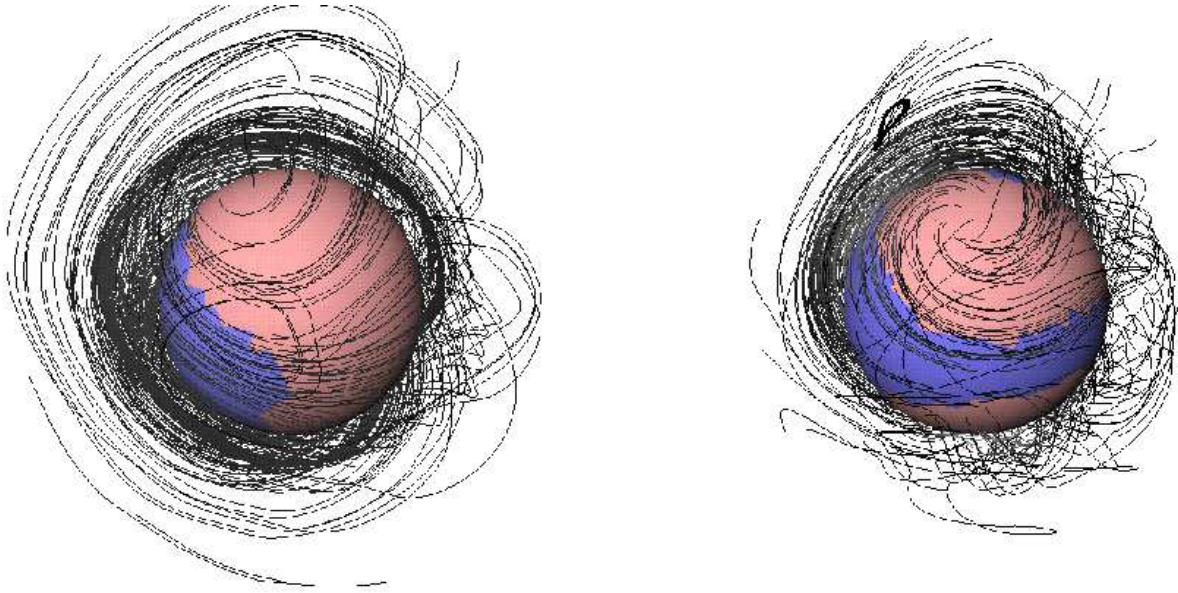


Fig. 12. Projections of the field lines without (left) and with (right) the field amplitude rescaling scheme (see Sect. 3.3), at a common time $t = 4.5$ days. Also plotted is a surface of constant radius $r = 0.4R_*$, which helps to provide a background against which to view the field lines.

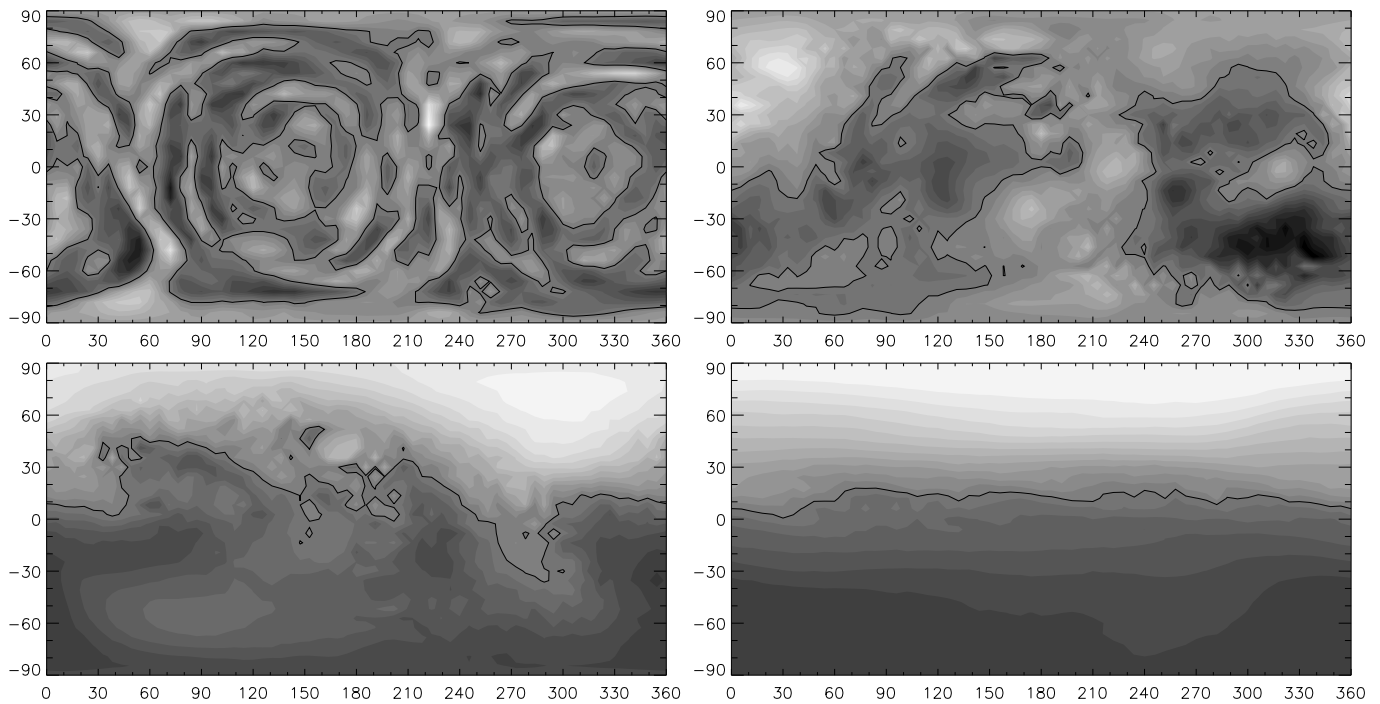


Fig. 17. Projections onto 2-D of the radial component B_r on the stellar surface, for the fiducial run at resolution 96^3 , at times $t = 0, 2.6, 9.8, 22.6$ days, using the axis M. The plots are arranged in the following order: top-left, top-right, upper-middle-left, upper-middle-right, etc.

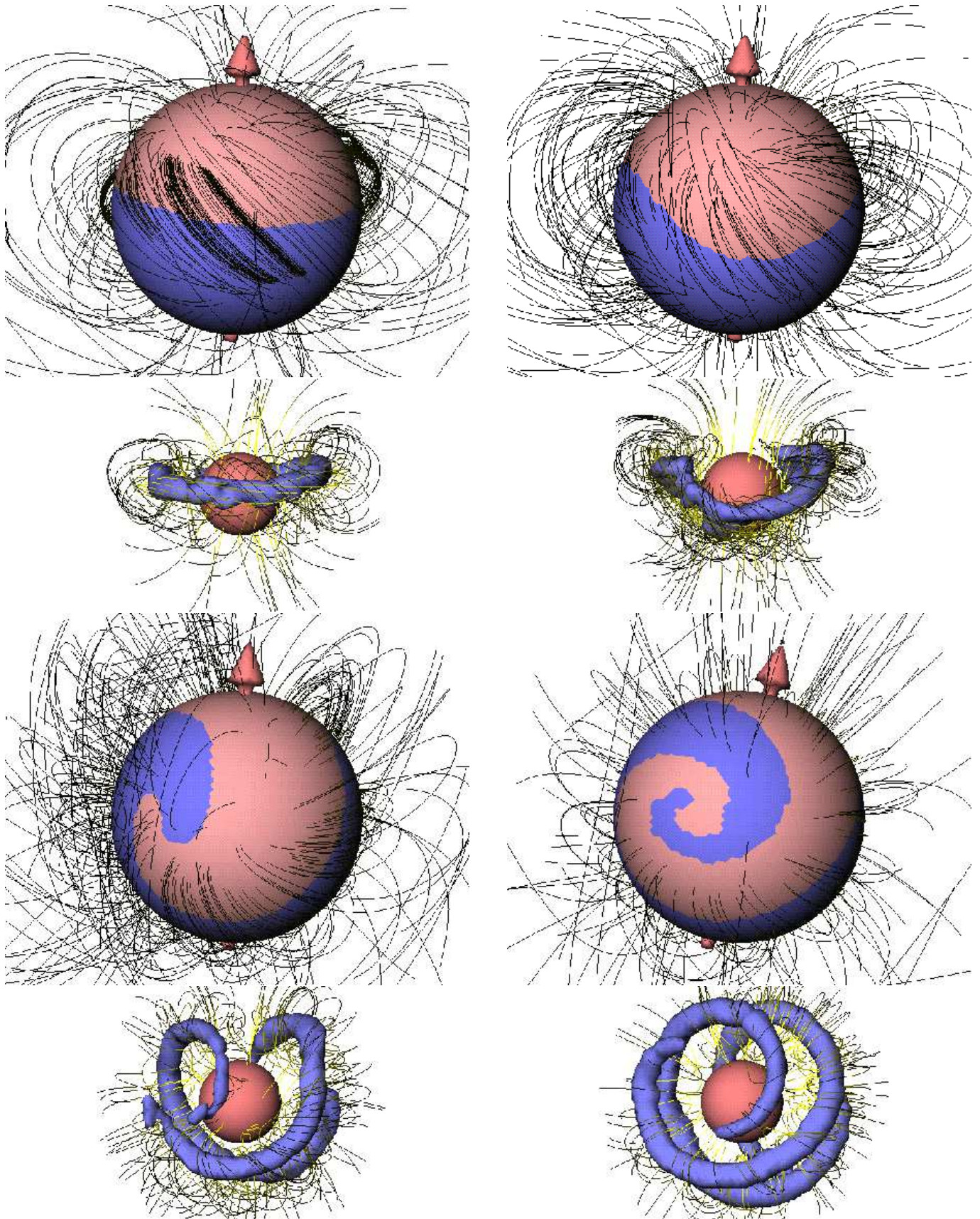


Fig. 20. Large plates: the magnetic field in the atmosphere of the star. The light and dark shading on the surface represent areas of positive and negative B_r , the radial component of the field. The arrow denotes the magnetic axis M calculated in Eq. (3). The four snapshots are taken at times $t = 31.9, 33.7, 35.6$ and 38.5 days; top-left, top-right, bottom-left, bottom-right respectively. In the first, the field has settled from the initial state into a fairly regular circular torus. In the next three we can see the instability grow (see Sect. 7.5). Small plates: at the same times, on the same scale, field lines in the stellar interior. To make it easier to trace their path, a surface of constant G (see Sect. 6 and Eq. (6)) has been added, as well as a sphere of radius $0.3R_*$.

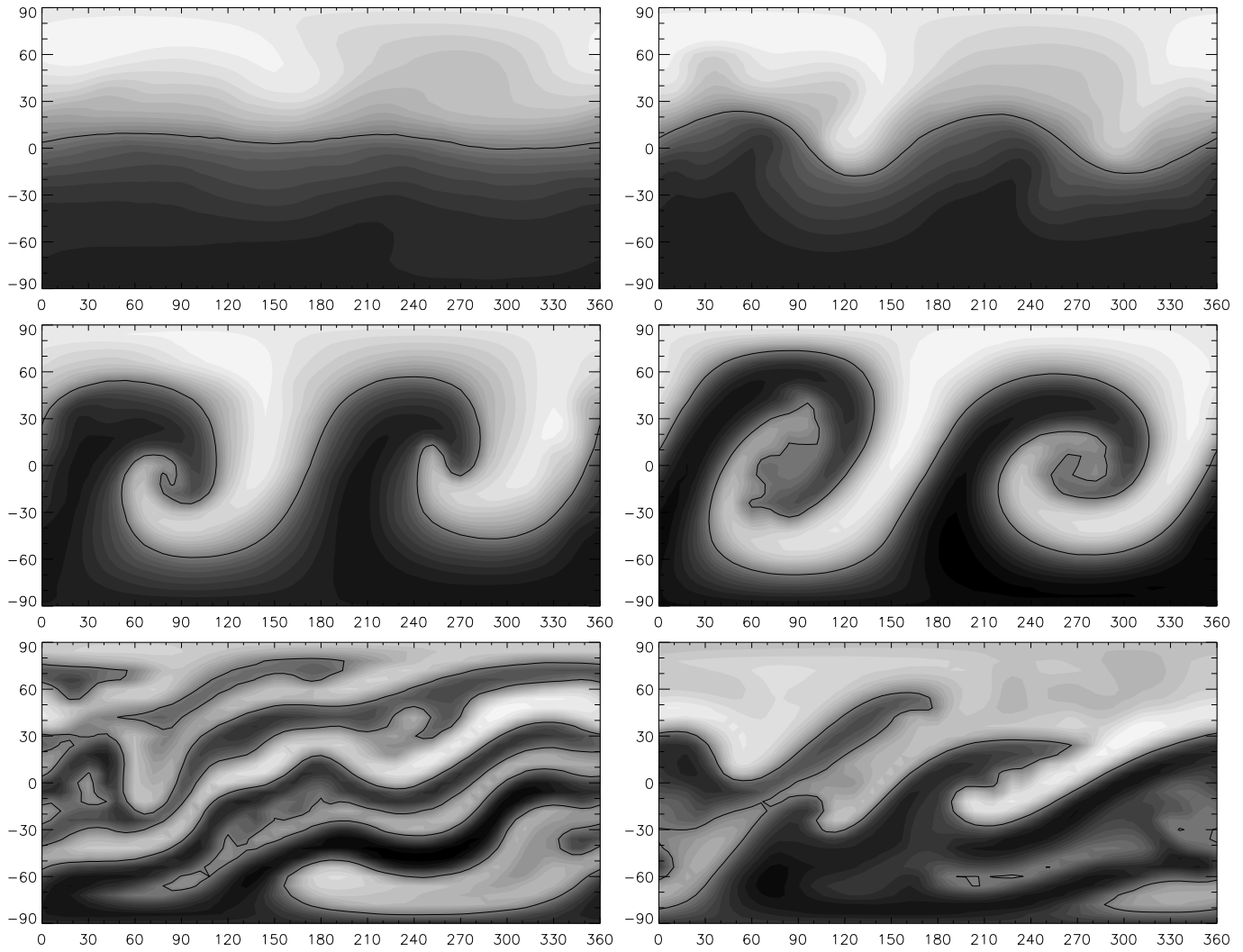


Fig. 21. Projections onto 2-D of the radial component B_r on the stellar surface, for the fiducial run at resolution 96^3 , at times $t = 31.9, 33.7, 35.6, 38.5, 43.2, 46.0$ days, using the axis M .

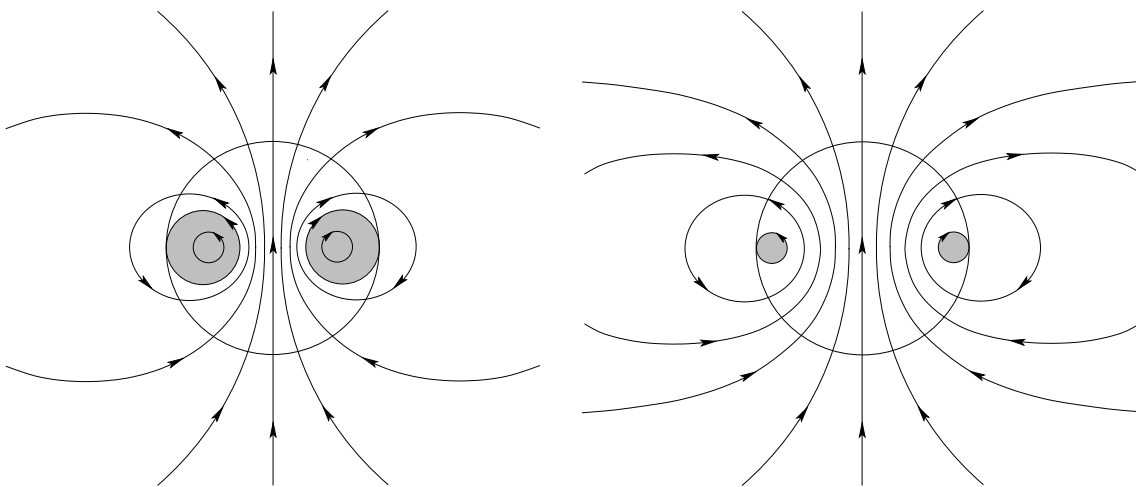


Fig. 24. Left: The toroidal field lines (represented by the shaded area) thread through those poloidal field lines which are closed within the star. Right: at a later time the field has diffused outwards and the toroidal component has been reduced compared to the poloidal.